Acta Crystallographica Section D
Biological Crystallography
ISSN 1399-0047

Structure of the ubiquitin-activating enzyme loaded with two ubiquitin molecules

Antje Schäfer, Monika Kuhn and Hermann Schindelin*

Structural Biology, Rudolf Virchow Center for Experimental Biomedicine, University of Würzburg, Josef-Schneider-Strasse 2, D-97080 Würzburg, Germany

Correspondence e-mail: hermann.schindelin@virchow.uni-wuerzburg.de

Received 6 December 2013
Accepted 9 February 2014

PDB reference: Uba1 in complex with ubiquitin-AMP and thioesterified ubiquitin, 4nnj

The activation of ubiquitin by the ubiquitin-activating enzyme Uba1 (E1) constitutes the first step in the covalent modification of target proteins with ubiquitin. This activation is a three-step process in which ubiquitin is adenylated at its C-terminal glycine, followed by the covalent attachment of ubiquitin to a catalytic cysteine residue of Uba1 and the subsequent adenylation of a second ubiquitin. Here, a ubiquitin E1 structure loaded with two ubiquitin molecules is presented for the first time. While one ubiquitin is bound in its adenylated form to the active adenylation domain of E1, the second ubiquitin represents the status after transfer and is covalently linked to the active-site cysteine. The covalently linked ubiquitin enables binding of the E2 enzyme without further modification of the ternary Uba1–ubiquitin$_2$ arrangement. This doubly loaded E1 structure constitutes a missing link in the structural analysis of the ubiquitin-transfer cascade.

1. Introduction

The covalent modification of proteins with ubiquitin triggers a variety of cellular activities in eukaryotic organisms. Besides the most common outcome of this modification, the targeted destruction of the labelled proteins by the proteasome, ubiquitylation also, for example, leads to altered cellular localization of proteins, promotes DNA repair and regulates transcription (van der Veen & Ploegh, 2012; Schulman & Harper, 2009). Malfunctions in the ubiquitylation machinery are linked to a variety of human diseases including cancer as well as neurodegenerative and metabolic disorders (Reinstein & Ciechanover, 2006; Goldberg, 2007; Petroski, 2008).

The activation of ubiquitin and its transfer to target proteins is carried out by a cascade consisting of three enzyme classes. (i) Ubiquitin-activating enzymes (E1) adenylate the C-terminus of ubiquitin and covalently bind ubiquitin *via* a thioester linkage (Haas & Rose, 1982; Haas *et al.*, 1982). (ii) Ubiquitin-conjugating enzymes (E2) interact with the E1 enzymes and accept ubiquitin *via* a transthioesterification reaction (Haas & Rose, 1982; Pickart & Rose, 1985). (iii) Ubiquitin ligases (E3) recognize the target proteins and transfer ubiquitin to specific lysine residues, leading to the formation of stable isopeptide bonds (Metzger *et al.*, 2012).

In addition to ubiquitin there are various small proteins, including SUMO and NEDD8 (van der Veen & Ploegh, 2012; Hänzelmann *et al.*, 2012), which are also used for post-translational modifications of macromolecules, thereby promoting distinct cellular activities. They are referred to as ubiquitin-like proteins (UBLs) and share the β-grasp fold with ubiquitin. Furthermore, UBLs are activated and conjugated *via* similar enzyme cascades. The activating enzymes and

ubiquitin-like proteins are derived from universally conserved systems (Burroughs *et al.*, 2009, 2012) and their prokaryotic homologues, for example, play a role in the biosynthesis of the molybdenum cofactor and thiamin (Rajagopalan, 1997; Rudolph *et al.*, 2001; Duda *et al.*, 2005; Lehmann *et al.*, 2006). The equivalents in these prokaryotic systems are MoaD and ThiS, which are folded like ubiquitin, and their homodimeric activating enzymes MoeB and ThiF, which resemble the active adenylation domain (AAD; see below).

The activation of ubiquitin is an essential step in eukaryotic organisms and is carried out in yeast by the ubiquitin-activating enzyme Uba1. Uba1 displays a complex architecture with an active and an inactive adenylation domain (AAD and IAD), a four-helix bundle (4HB), a domain carrying the active-site cysteine, which can be subdivided into two smaller units (the first and second catalytic cysteine half domains; FCCH and SCCH, respectively), and a C-terminal ubiquitin-fold domain (UFD) (Lee & Schindelin, 2008; Hänzelmann *et al.*, 2012; Olsen & Lima, 2013). All known eukaryotic E1 enzymes share this general domain architecture, including the SUMO and NEDD8 activating enzymes, which form a heterodimeric assembly derived from two polypeptides (Walden *et al.*, 2003; Lois & Lima, 2005; Huang *et al.*, 2007). In the last decade crystal structures of the activating enzymes for ubiquitin and the UBLs SUMO and NEDD8 have been reported in various functional states, as well as structures of the MoeB–MoaD (Lake *et al.*, 2001) and ThiF–ThiS complexes (Duda *et al.*, 2005; Lehmann *et al.*, 2006). With respect to the ubiquitin-activating enzyme Uba1, structures of binary E1–ubiquitin complexes from *Saccharomyces cerevisiae* and *Schizosaccharomyces pombe* have been reported (Lee & Schindelin, 2008; Olsen & Lima, 2013). In addition, a ternary complex consisting of the *S. pombe* E1 bound noncovalently to ubiquitin and the ubiquitin-conjugating enzyme Ubc4 in which the E1 and E2 active-site cysteines were chemically cross-linked has been described (Olsen & Lima, 2013). Regarding the formation of an E1–UBL acyladenylate, multiple E1 structures exist which contain Mg^{2+}–ATP prior to hydrolysis, but the formation of a UBL–AMP conjugate bound to an E1 enzyme has never been observed before.

The mechanism of the ubiquitin (SUMO/NEDD8) activating enzymes is a three-step process. The UBL protein is bound together with Mg^{2+}–ATP at the AAD, where it is adenylated. In a series of conformational changes the active-site cysteine attacks the acyladenylate (Olsen *et al.*, 2010), resulting in the formation of the thioester linkage and presumably dragging the UBL protein away from the AAD when the active-site cysteine resumes its initial position. In a subsequent step a second UBL protein is adenylated so that under steady-state conditions two UBL proteins are bound to the E1: one noncovalently at the AAD and the other *via* a thioester linkage to the active-site cysteine (Ciechanover *et al.*, 1981; Haas *et al.*, 1982). In the case of the ubiquitin-activating enzyme the bound ubiquitin molecules are referred to as Ub(a) and Ub(t), respectively. The E1 is now ready to interact with E2 enzymes to transfer the covalently bound UBL protein to the E2 active-site cysteine. Here, we present a crystal structure of a ternary Uba1–Ub_2 complex in which one ubiquitin is bound as an acyladenylate at the AAD while the second ubiquitin is covalently linked to the active-site cysteine, thus representing the state of E1 immediately prior to E2 binding.

2. Materials and methods

2.1. Protein expression and purification

For the expression of N-terminally hexahistidine-tagged Uba1 from *S. cerevisiae*, the previously described pET28a-UBA1 construct containing the coding sequence for residues 10–1024 was used (Lee & Schindelin, 2008). The coding sequences for ubiquitin and Ubc6* (amino acids 1–171, where the asterisk indicates the catalytically inactive C112A variant) from *S. cerevisiae* were cloned into pETM11 (EMBL, Heidelberg, Germany). For enhanced TEV cleavage of His_6-ubiquitin, an additional sequence coding for the amino acids Ser-Ala-Ala was introduced between the TEV-cleavage site and the start codon of the open reading frame, yielding the pETM11-SAA-Ub plasmid.

His_6-Uba1, His_6-ubiquitin and His_6-Ubc6* were expressed in *Escherichia coli* BL21(DE3) RIL cells (Novagen) by induction with 0.3 m*M* IPTG at an OD_{600} of 0.6–1 followed by overnight growth at 16°C. Uba1 was purified as described previously (Lee & Schindelin, 2008). Ubiquitin and Ubc6* were purified in buffer *A* [50 m*M* Tris pH 7.5, 500 m*M* NaCl, 10%(*w*/*v*) glycerol, 20 m*M* imidazole, 5 m*M* β-mercaptoethanol] by nickel-affinity chromatography (Ni–NTA, Invitrogen) and size-exclusion chromatography (HiLoad Superdex 200 26/60, GE Healthcare) in buffer *B* (25 m*M* Tris pH 7.5, 150 m*M* NaCl, 5 m*M* β-mercaptoethanol). Prior to size-exclusion chromatography, His_6-ubiquitin and His_6-Ubc6* were dialyzed in buffer *B* at 4°C overnight in the presence of TEV protease followed by Ni–NTA chromatography to remove uncleaved proteins as well as His-tagged TEV protease. The proteins were concentrated by ultrafiltration (Vivaspin, Sartorius) to 20–30 mg ml^{-1} for His-Uba1 and 6–8 mg ml^{-1} for ubiquitin and Ubc6*, shock-frozen in liquid nitrogen and stored at −80°C.

2.2. Analytical size-exclusion chromatography

To observe the formation of an E1–Ub_2 complex, 44 μ*M* Uba1 was incubated with 88 μ*M* ubiquitin in the presence of 2.5 m*M* ATP and 5 m*M* $MgCl_2$. As a control, 44 μ*M* Uba1 mixed with 88 μ*M* ubiquitin was used. Each reaction mixture was subjected to analytical size-exclusion chromatography (Superdex 200 5/150 GL, GE Healthcare).

2.3. Native gel mobility shift assay

Native agarose gel electrophoresis was carried out as described by Kim *et al.* (2000) using a horizontal gel chamber (Bio-Rad Laboratories, Germany). A 0.8% agarose gel was prepared in 25 m*M* Tris–HCl pH 8.5, 19.2 m*M* glycine and electrophoresis was performed at a constant voltage of 50 V for 7 h at 4°C. 43 μ*M* Uba1 ± Mg^{2+}–ATP and 43 μ*M* Uba1 +

86 µ*M* ubiquitin ± Mg^{2+}–ATP (5 m*M* $MgCl_2$, 2.5 m*M* ATP) were incubated for 1 h at room temperature and were mixed with sample buffer (20% glycerol, 0.2% bromophenol blue, 0.12 *M* Tris base) in a 1:1 ratio prior to loading. Gels were stained with Coomassie Brilliant Blue R.

2.4. Crystallization

For crystallization, purified His_6-Uba1, ubiquitin and Ubc6* were incubated at a molar ratio of 1:2:1 for 1 h at room temperature in the presence of 2.5 m*M* ATP and 5 m*M* $MgCl_2$ with a final total protein concentration of 15 mg ml^{-1}. Crystals were grown by vapour diffusion at 20°C in 1 µl hanging drops containing equal volumes of protein in buffer (25 m*M* Tris pH 7.5, 150 m*M* NaCl, 5 m*M* β-mercaptoethanol) and a reservoir solution consisting of 15%(*w*/*v*) polyethylene glycol 3350, 0.2 *M* lithium sulfate, 0.1 *M* bis-tris pH 6.0 equilibrated against 1 ml reservoir solution. Crystals belonged to the orthorhombic space group $P22_12_1$, with unit-cell parameters a = 73.0, b = 195.6, c = 230.6 Å. Despite being present in the protein mixture employed for crystallization, Ubc6* was not present in the crystals.

2.5. Data collection and structure determination

Crystals were cryoprotected by soaking in mother liquor containing 15%(*v*/*v*) glycerol and were then flash-cooled in liquid nitrogen. Data collection was performed at 100 K either on the BL14.1 beamline at BESSY, Berlin, Germany or the ID23.2 beamline at ESRF, Grenoble, France, and the data were processed using *XDS* and *SCALA* (Evans, 2006; Kabsch, 2010). Data-collection statistics are summarized in Table 1. For the initial molecular replacement *Phaser* (McCoy *et al.*, 2007) was used with one Uba1–Ub complex (chains *A* and *B* of PDB entry 3cmm; Lee & Schindelin, 2008) as a search model, identifying two complexes. The third ubiquitin molecule was built manually into the remaining electron density using *Coot* (Emsley & Cowtan, 2004). Structural refinement employing NCS and reference-model restraints was carried out using *PHENIX* v.1.8-1069 (Adams *et al.*, 2010). Simulated-annealing OMIT maps for adenylated and thioesterified ubiquitin molecules were calculated in *PHENIX* by omitting the respective ubiquitin molecule from the original model and using Cartesian dynamics in combination with an annealing temperature of 3000 K. Figures containing protein structures were created with *PyMOL* (http://www.pymol.org). All interfaces were analysed using *PDBePISA* (Krissinel & Henrick, 2007).

3. Results and discussion

For the activation of ubiquitin by the E1 enzyme Uba1, ubiquitin (Ub) is bound first to the active adenylation domain (AAD) of Uba1, where it is conjugated *via* a mixed anhydride linkage to AMP derived from ATP in the presence of Mg^{2+} (Haas *et al.*, 1983). Ubiquitin is recruited to *S. cerevisiae* Uba1 even in the absence of Mg^{2+}–ATP, as observed in the previously reported E1 structure (Lee & Schindelin, 2008).

Table 1
Data-collection and refinement statistics.

Values in parentheses refer to the last shell.

Data-collection statistics	
Space group	$P22_12_1$
Unit-cell parameters (Å)	a = 73.0, b = 195.6, c = 230.6
Complexes per asymmetric unit	2
X-ray source	ID23.2, ESRF
Wavelength (Å)	0.873
Resolution limits (Å)	90.0–2.4
No. of observations	645480
No. of unique observations	127962
Completeness (%)	98.9 (93.4)
R_{merge} (%)	9.3 (112.0)
$R_{p.i.m.}$ (%)	4.4 (70.8)
$\langle I/\sigma(I)\rangle$	11.7 (1.0)
$CC_{1/2}$ (%)	99.7 (53.4)
Mean multiplicity	5.0 (3.2)
Refinement statistics	
Resolution (Å)	48.68–2.4
No. of protein/solvent atoms	17798/1272
R/R_{free} (%)	16.4/20.1
Root-mean-square (r.m.s.) deviations	
Bond lengths (Å)	0.011
Bond angles (°)	1.352
Chiral volumes (Å^3)	0.070
Planar groups (Å)	0.006
Wilson B factor (Å^2)	40.1
Average B factors (Å^2)	
Protein atoms	53.3
Solvent atoms	45.1
Uba1	51.6
Ub(a)	58.4
Ub(t)	94.2
Ramachandran statistics (%)	
Favoured	96.82
Allowed	2.86
Outliers	0.31
Coordinate error (Å)	0.29

After adenylating the C-terminal glycine residue of Ub, this entity is covalently linked to the side chain of the E1 catalytic residue (Cys600 of *S. cerevisiae* Uba1), yielding an E1–Ub thioester and free AMP. Subsequently, a second ubiquitin can bind to the AAD (Huang *et al.*, 2007; Haas *et al.*, 1982). The Uba1 complex loaded with two ubiquitin molecules can be visualized by a slightly slower migration in native agarose gels after electrophoresis compared with Uba1 and the Uba1–Ub complex (Fig. 1*a*). This is additionally corroborated by the moderately smaller elution volume of the Uba1–Ub_2 complex in analytical size-exclusion chromatography (aSEC) experiments, consistent with a higher molecular-weight complex in comparison to Uba1 bound to just one ubiquitin (Fig. 1*b*). The addition of an E2 enzyme such as the yeast ubiquitin-conjugating enzyme Ubc6* to the Uba1–Ub_2 complex partially led to the formation of a Uba1–Ub_2–Ubc6* complex (data not shown). Ubc6* was comprised of residues 1–171 and carried a mutation in the active-site cysteine (C112A). Therefore, the transfer of activated ubiquitin from Uba1 to Ubc6* was prevented, thus resulting in a stable Uba1–Ub_2–Ubc6* complex. It was our original goal to crystallize this quaternary complex consisting of an E1 enzyme, an E2 enzyme and two ubiquitin molecules.

Using *in vitro* pre-formed Uba1–Ub_2–Ubc6* complex, we obtained crystals with plate morphology (Fig. 1*c*) belonging to

the orthorhombic space group $P22_12_1$ (Table 1). With the aid of molecular replacement using the Uba1–Ub structure of *S. cerevisiae* (PDB entry 3cmm, chains *A* and *B*), two copies of the Uba1–Ub complex could be placed in the asymmetric unit in a heterotetrameric arrangement. An initial examination of the resulting maps revealed the presence of significant electron-density features corresponding to (i) two AMP moieties, each covalently linked to Gly76 of the ubiquitin chains (Figs. 2*a* and 2*c*), and (ii) extended electron density corresponding to another ubiquitin molecule (Fig. 2*b*). Attempts to localize this ubiquitin chain by molecular replacement failed, presumably owing to its higher mobility, as reflected by the average *B* factors (Table 1), and its small size compared with the content of the asymmetric unit. Hence, the density was manually interpreted as a single Ub chain (Fig. 2*b*). The C-terminus (residues 73–75) of the additional Ub chain exhibits poor electron density. Nevertheless, it is covalently linked with its C-terminal Gly76 *via* a thioester bond to the side chain of Cys600, as demonstrated by electron density in simulated-annealing maps after omitting the Ub(t) molecule (Figs. 2*b* and 2*d*).

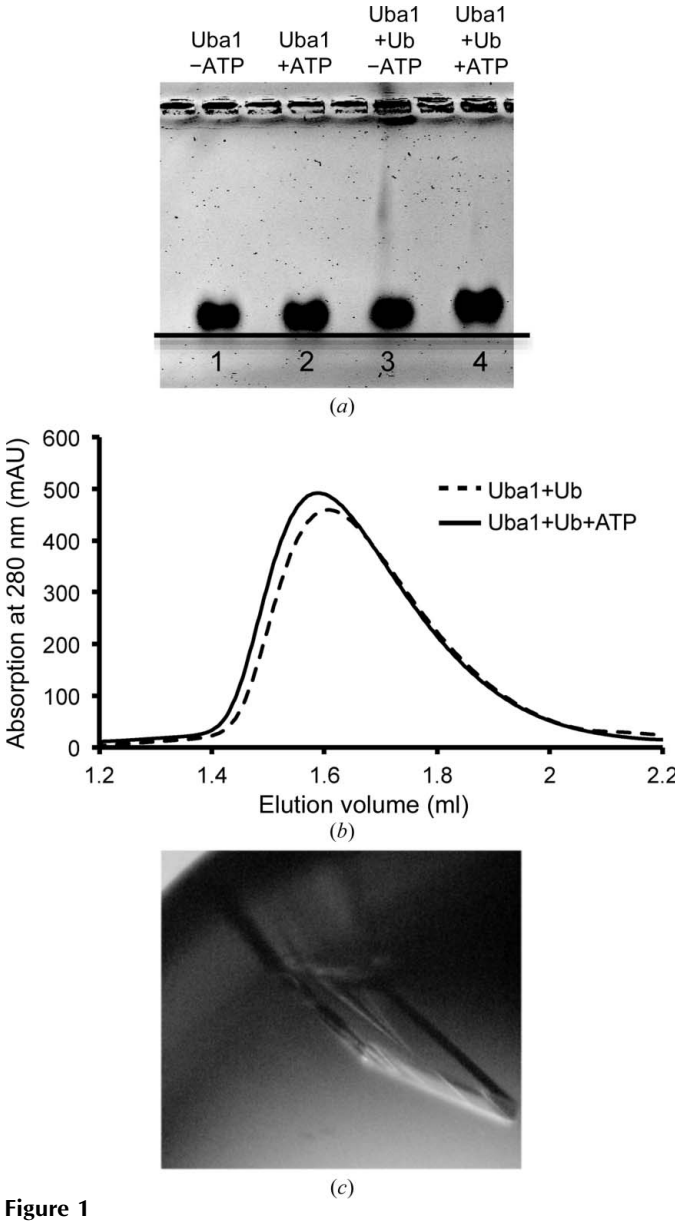

Figure 1
Biochemical characterization of the Uba1–Ub_2 complex. (*a*) Native agarose gel electrophoresis documenting different migration patterns for Uba1 without Mg^{2+}–ATP (lane 1), Uba1 with Mg^{2+}–ATP (lane 2), Uba1–Ub without Mg^{2+}–ATP (lane 3) and Uba1–Ub with Mg^{2+}–ATP representing the Uba1–Ub_2 complex (lane 4). (*b*) Analytical size-exclusion chromatography of Uba1–Ub (dashed line) and Uba1–Ub with Mg^{2+}–ATP–ATP (solid line). (*c*) Crystals of the ternary Uba1–Ub_2 complex with approximate dimensions of 60 × 70 × 10 µm.

The thioester-linked ubiquitin [Ub(t)] is observed solely in one of the two Uba1 complexes (Fig. 3*a*). This appears to be owing to crystal contacts mediated by Uba1 symmetry mates favourably interacting with Ub(t), thus leading to its visibility in the electron-density maps (Supplementary Fig. S1[1]). At the same time, crystal packing prevents the presence of Ub(t) in the second Uba1 complex (Fig. 3*a*, circle). The structure was refined to *R* and R_{free} values of 0.164 and 0.201, respectively, at 2.4 Å resolution utilizing torsion-angle NCS and reference-model restraints and exhibits good stereochemical parameters (Table 1). Although included in the crystallization setup, Ubc6* was not present in the crystals. The absence of Ubc6* can be explained by the fact that the pre-formed protein mixture used for crystallization contained a mixture of Uba1–Ub_2–Ubc6* (minor component) and the Uba1–Ub_2 complex (major component).

The overall structure of Uba1 in this complex (Fig. 3*b*; PDB entry 4nnj) displays the well known six structural domains IAD, AAD, FCCH, SCCH, 4HB and the C-terminal UFD domain as described before (Lee & Schindelin, 2008; Olsen & Lima, 2013). The SCCH and AAD domains are connected by a stretch of residues in extended conformation which is referred to as the crossover loop. The catalytic Cys600 is masked by the Cys CAP loop comprised of residues 776–784. In addition, one ubiquitin-adenylate [Ub(a)] is bound to the AAD and one ubiquitin molecule resides covalently bound to the catalytic Cys domain. This thioesterified ubiquitin [Ub(t)] is located on the same side as Ub(a) (Fig. 3*b*) but is displaced by roughly 31 Å as measured by the shift in the centre of gravity with *LSQKAB*/*SUPERPOSE* (Kabsch, 1976, 1978; Krissinel & Henrick, 2004). The buried interface between Ub(t) and Uba1 amounts to an area of ∼900 $Å^2$ or ∼18% of the total Ub(t) surface area (∼5000 $Å^2$), while Ub(a) bound to the AAD buries a surface area of ∼1600 $Å^2$, which corresponds to about 33% of the total ubiquitin surface calculated with *PDBePISA* (Krissinel & Henrick, 2007). This suggests that Ub(t) is not bound as tightly to Uba1 as Ub(a), which is also reflected by the significantly higher *B* factors of Ub(t) (Table 1). Despite its high *B* factors Ub(t) makes a substantial contribution to the overall model since its omission from the final model resulted in an increase in *R* and R_{free} from 0.164 and 0.201 to 0.178 and 0.212, respectively. In comparison, omission of either of the Ub(a) moieties increased *R* and R_{free} to 0.191 and 0.231 or to 0.193 and 0.225, respectively.

[1] Supporting information has been deposited in the IUCr electronic archive (Reference: BE5254).

The covalent linkage between Uba1 and Ub(t) of course prevents the rapid dissociation of Ub(t), yet the less tight binding of Ub(t) would allow efficient transfer to a bound E2 enzyme. Besides the covalent linkage between Cys600 in the SCCH and Gly76, contacts between Uba1 and Ub(t) are mainly enabled by the FCCH (Figs. 3*c* and 3*d*). The following residues are involved in these interactions: Lys6, Arg42, Ile44, His68, Leu73, Gly76 of ubiquitin and Asp188, Asp200 and Phe236 of Uba1 (Fig. 3*b*). Residues Asp200 and Phe236 are type-conserved among Uba1 enzymes of various organisms, thus underscoring that the interaction with Ub(t) as observed in the crystal structure corresponds to a functional state. The participation of Ile44 seems remarkable as this residue constitutes the hydrophobic patch of ubiquitin which is involved in many interactions of Ub with other proteins, including the binding of Ub(a) to Uba1. In a previously

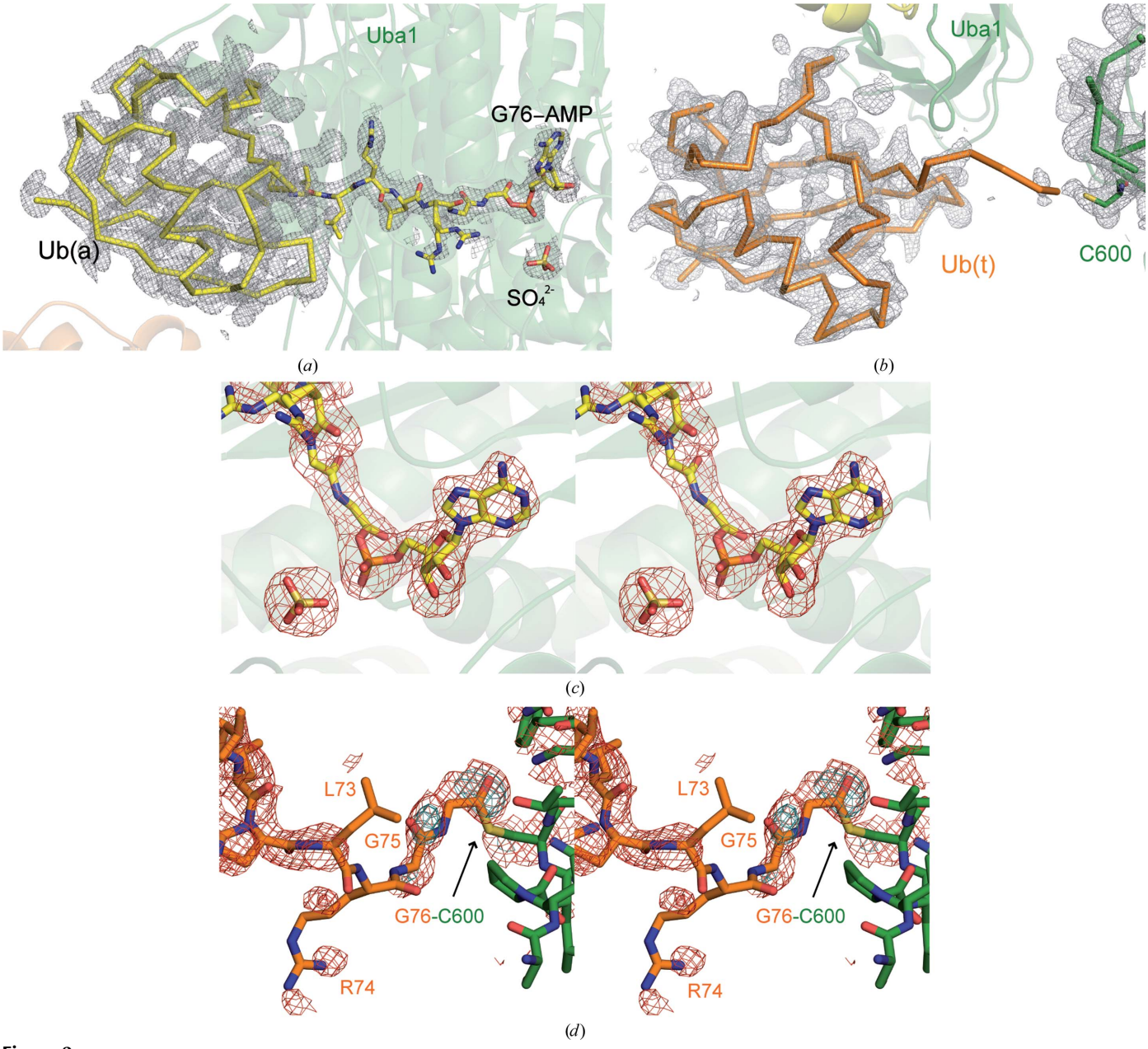

Figure 2
Simulated-annealing OMIT maps of the adenylated and covalently bound ubiquitin molecules. (*a*) Simulated-annealing $2F_o - F_c$ OMIT map contoured at an r.m.s. deviation of 1 (grey mesh) for adenylated ubiquitin, Ub(a) (PDB entry 4nnj, chain *D*), coloured in yellow. The Uba1 molecule is coloured transparent green. (*b*) Simulated-annealing $2F_o - F_c$ OMIT map (grey mesh) of the covalently linked ubiquitin (orange), Ub(t) (chain *E*), at an r.m.s. deviation of 1. (*c*) Detailed stereoview of the linkage between the C-terminal Gly76 of ubiquitin and AMP. The corresponding simulated-annealing $F_o - F_c$ map is contoured at an r.m.s. deviation of 3 and is coloured in red. (*d*) Close-up view of the thioester linkage between the C-terminal Gly76 of Ub(t) and the catalytic Cys600 of Uba1 shown in stereo. The simulated-annealing $F_o - F_c$ map (red mesh) is contoured at an r.m.s. deviation of 2 to reveal some density for the highly mobile residues 73–75 of Ub(t). Difference density in the immediate vicinity of Cys600, which represents the carboxy moiety of Gly76, is clearly visible at an r.m.s. deviation of 3 (cyan mesh).

reported structure of the heterodimeric E1 enzyme APPBP1-UBA3 doubly loaded with two ubiquitin-like NEDD8 molecules (Huang *et al.*, 2007), the NEDD8(a) molecule bound to AAD buries 32% of its surface area, which is of comparable size to the Uba1–Ub(a) interface. In contrast, the NEDD8(t) molecule shows even less contact with APPBP1-UBA3 than Ub(t) with Uba1 (burying only ∼7.5% of its surface area). This smaller area is offset by additional interactions between NEDD8(t) and Ubc12, the E2 specific for NEDD8. It is conceivable that similar E2–Ub(t) interactions are present in the quaternary Uba1–Ub_2–Ubc complex (see below).

Comparison of both Uba1 complex structures in the asymmetric unit with the previously reported molecules from *S. cerevisiae* and *S. pombe* (PDB entries 3cmm and 4ii2; Lee & Schindelin, 2008; Olsen & Lima, 2013) show a similar overall topology (Figs. 4*a*, 4*b* and 4*c*). However, the orientation of the UFD domains varies between the Uba1 molecules owing to a

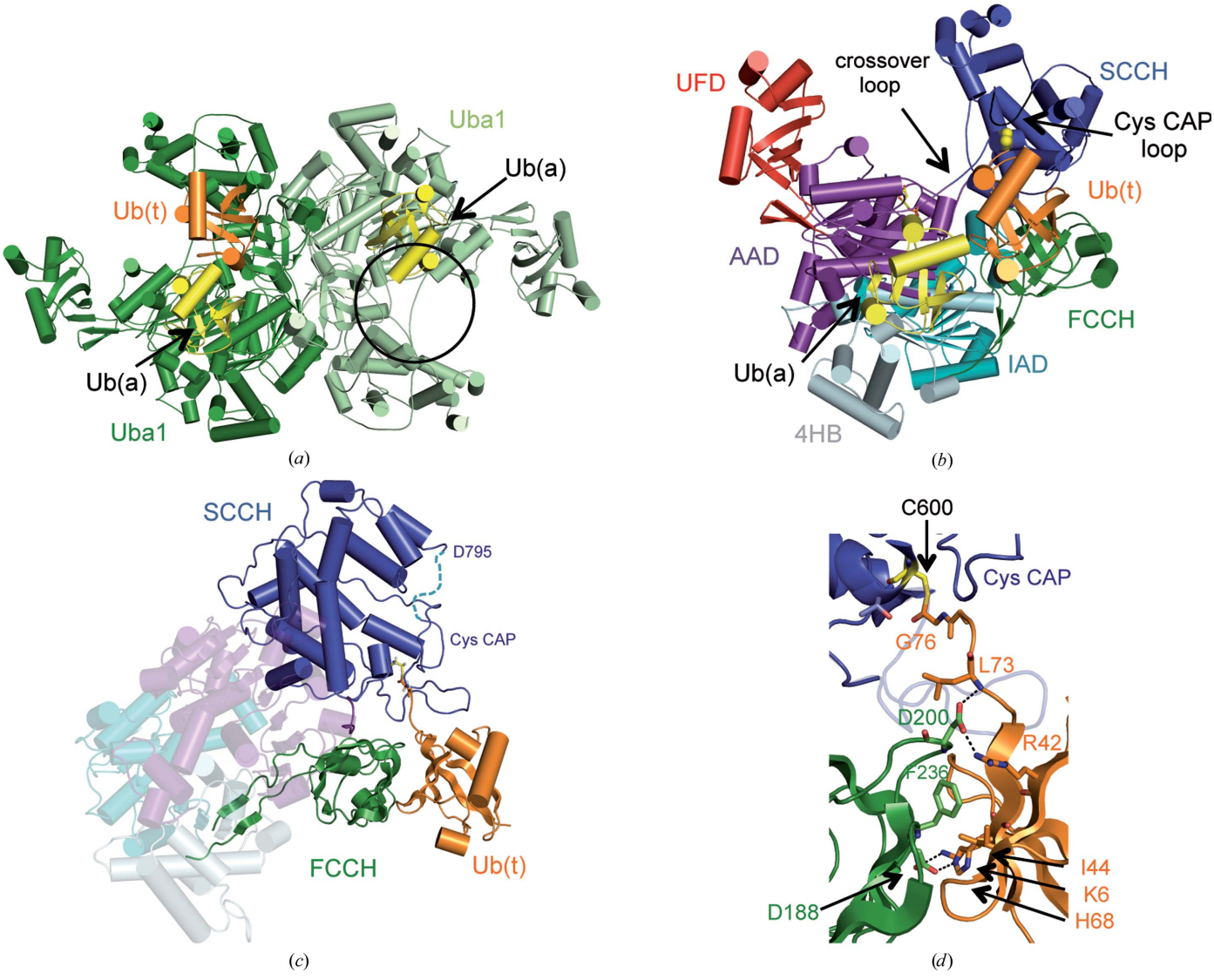

Figure 3
Structure of the Uba1–Ub_2 complex and representation of the contacts between Uba1 and Ub(t). (*a*) Content of the asymmetric unit featuring two Uba1 molecules (dark and light green), two Ub(a) chains (yellow) and one Ub(t) chain (orange). α-Helices are presented as cylinders and β-strands as arrows. The corresponding position for the second Ub(t) is vacant (black circle). (*b*) Overall structure of the Uba1–Ub_2–AMP complex coloured as described below. Uba1 is comprised of six domains: AAD in purple, IAD in cyan (active and inactive adenylation domains), 4HB in pale cyan, FCCH in green, SCCH in blue (the first and second catalytic cysteine half domains) and the C-terminal ubiquitin-fold domain in red (UFD). The crossover loop connects the SCCH to the AAD domain. The adenylated form of ubiquitin Ub(a) is coloured yellow and the thioesterified Ub(t) is coloured orange, which is linked to the catalytic Cys600 (yellow spheres) of Uba1. The Cys CAP loop (black) masks Cys600. (*c*) Top view of the overall Uba1–Ub(t) arrangement colour-coded as in (*b*). The Uba1 domains which are not involved in Ub(t) binding are rendered more transparent and the UFD has been removed for clarity. Uba1–Ub(t) contacts are mainly mediated by the FCCH domain (green). Amino acids 787–795 in the SCCH lack visible density and are connected by a dashed line. (*d*) Detailed view of the interface presented in (*c*). Besides the covalent linkage between Cys600 of Uba1 (yellow) and Gly76 of Ub(t), the indicated residues Lys6, Arg42, Ile44, His68 and Leu73 of ubiquitin and Asp188, Asp200 and Phe236 of Uba1 mediate this interaction. Hydrogen bonds are indicated as dashed lines.

hinge motion. The UFD of the Uba–Ub_2 complex (PDB entry 4nnj, chains *A* and *C*) fits exactly to the UFD of one of the Uba1 molecules of *Sc*Uba1–Ub (PDB entry 3cmm, chain *A*) and to both molecules of *Sp*Uba1–Ub (PDB entry 4ii3; Olsen & Lima, 2013). This orientation is supposed to be the 'distal' or 'unlocked' conformation of the UFD (Olsen & Lima, 2013), in which Uba1 is able to interact with an E2 ubiquitin-conjugating enzyme. In Uba1 from *S. pombe* (Olsen & Lima, 2013) a rotation by 25° from the distal to a proximal conformation is observed after binding of the E2 enzyme Ubc4 (Figs. 4*c* and 4*d*). Besides these distal and proximal orientations of the UFD domains, the superposition of the Uba1–Ub complexes of all other known *S. cerevisiae* structures also displays intermediate conformations of the UFD, which might be generated by lattice contacts or might represent variations of the initial distal UFD conformation (Fig. 4*d*).

Although the E1 enzyme should adenylate ubiquitin in the presence of ATP and Mg^{2+}, leading to a covalent AMP linkage, the adenylated derivative of ubiquitin has not been observed so far. Besides the published Uba1–Ub structure from *S. cerevisiae*, in which no ATP was present in the crystallization setups (Fig. 5*a*, left), all other E1 enzymes including *S. pombe* Uba1 (Fig. 5*b*, left) and the human E1 enzymes for SUMO and NEDD8 exclusively show ATP and Mg^{2+} close to the C-terminal glycine residue of ubiquitin or the ubiquitin-like protein (Lee & Schindelin, 2008; Olsen & Lima, 2013; Lois & Lima, 2005; Walden *et al.*, 2003; Huang *et al.*, 2007). In the Uba1 structure presented here the ubiquitin–AMP intermediate can be easily resolved in both complexes of the asymmetric unit (Figs. 2*c* and 5*c*, left). In addition to electron density of the AMP moiety, we observed secondary density features, which we have modelled as sulfate owing to the presence of 0.2 *M* Li_2SO_4 in the crystallization conditions. This sulfate could indicate the position of the pyrophosphate leaving group, as it coincides with the position of the γ-phosphate of ATP (Fig. 5*b* *versus* Fig. 5*c*).

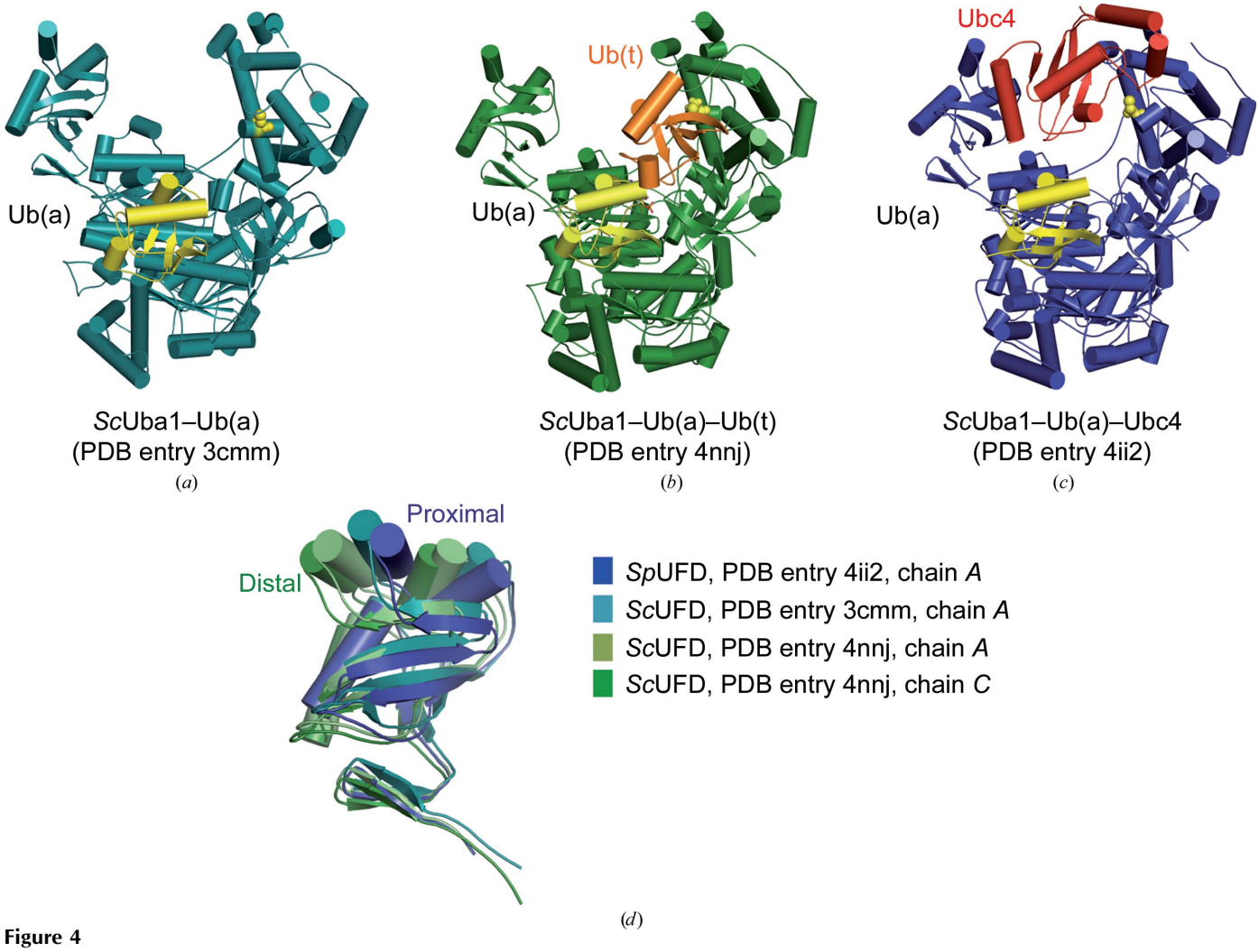

Figure 4
Comparison of known Uba1 structures. Overall structures of Uba1 enzymes loaded with Ub(a) coloured in yellow at the AAD. The respective active-site cysteine residues are shown as yellow spheres. (*a*) *S. cerevisiae* Uba1–Ub(a) with Uba1 in cyan (PDB entry 3cmm), (*b*) *S. cerevisiae* Uba1–Ub(a)–Ub(t) with Uba1 in green and Ub(t) in orange (PDB entry 4nnj) and (*c*) *S. pombe* Uba1–Ub(a)–Ubc4 with Uba1 in blue and Ubc4 in red (PDB entry 4ii2). (*d*) Superposition of the UFD conformations shown in (*b*) (PDB entry 4nnj, chain *C*) and (*c*) (PDB entry 4ii2, chain *B*), illustrating the transition between proximal (blue) and distal (dark green) states. The second molecule present in the asymmetric unit in both Uba1 structures from *S. cerevisiae* displays an intermediate conformation even without binding of an E2 and is coloured pale green (PDB 4nnj, chain *A*) or cyan (PDB entry 3cmm, chain *A*).

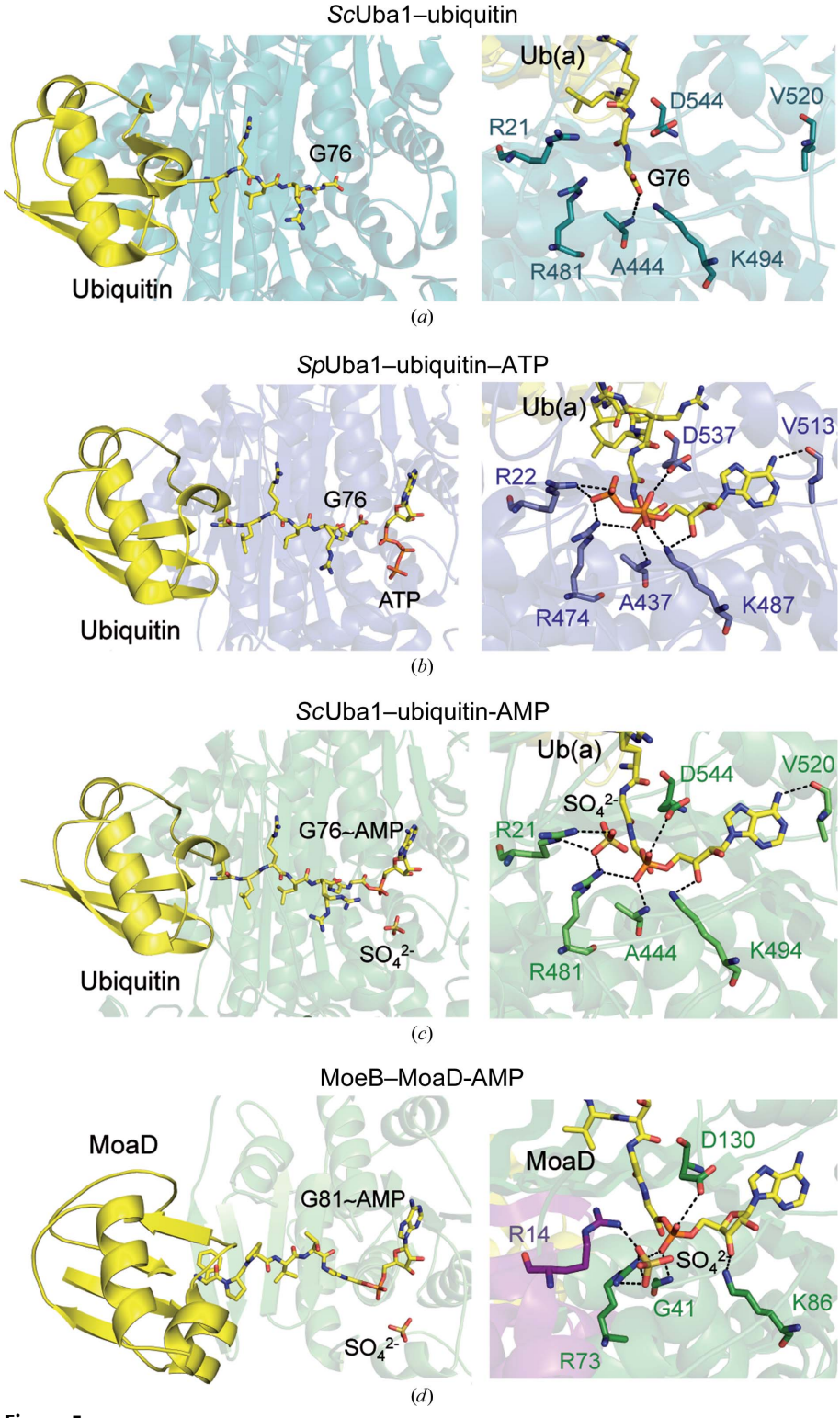

Figure 5
The ubiquitin-adenylate in comparison to other Ub(a) structures and the MoaD-adenylate. In the left panels an overview of the UBL (yellow) is shown bound to the respective activating enzymes colour-coded as described in Fig. 4 but rendered with a higher transparency. The right panels show a detailed view of the respective adenylation active site including critical residues. Hydrogen bonds are indicated as dashed lines. Structures of (*a*) Uba1–Ub from *S. cerevisiae* in the absence of ATP (PDB entry 3cmm), (*b*) Uba1–Ub–ATP from *S. pombe* (PDB entry 4ii3), (*c*) Uba1–Ub(a)–Ub(t) from *S. cerevisiae* including the ubiquitin-adenylate (PDB entry 4nnj) and (*d*) *E. coli* MoeB–MoaD including the MoaD-adenylate (PDB entry 1jwb). MoeB is coloured green, while the second MoeB monomer in the heterotetrameric MoaB–MoaD structure and the critical Arg14 are coloured purple.

Our structure represents the first E1 enzyme in which an acyladenylate has been formed at the C-terminus of the UBL. The only related structure displaying this feature (PDB entry 1jwb) is the MoeB–MoaD–AMP complex from *E. coli* (Lake *et al.*, 2001). Despite the lack of significant sequence similarity in comparison to eukaryotic UBLs, MoaD displays the same fold as ubiquitin and is activated at its C-terminus by the homodimeric enzyme MoeB. The conformations of the Gly-Gly adenylate and the key catalytic residues are remarkably similar between MoeB–MoaD–AMP and our Uba1–Ub–AMP structure (Figs. 5*c* and 5*d*, right). The conserved residues Gly41, Arg73, Lys86 and Asp130 of MoaB involved in AMP binding (Fig. 5*d*, right) correspond to Ala444, Arg481, Lys494 and Asp544 in *Sc*Uba1 (Fig. 5*c*, right), respectively. However, there is no equivalent hydrogen bond in the MoeB–MoaD–AMP complex involving the exocyclic amino group of the base and a main-chain O atom like Val520 in *Sc*Uba1 or Val513 in *Sp*Uba1 (Figs. 5*a*, 5*b* and 5*c*, right). In addition, the MoeB–MoaD complex also features a sulfate ion derived from the mother liquor at the presumed position of the pyrophosphate leaving group (Fig. 5*d*). In the heterotetrameric structure of MoeB–MoaD, Arg14 of the second MoeB monomer participates in the stabilization of the pyrophosphate leaving group generated at the first MoaB monomer (Fig. 5*d*, right). Arg14 is crucial for MoaB activity and its counterparts in yeast are Arg21 in *S. cerevisiae* (Fig. 5*c*, right) and Arg22 in *S. pombe* (Fig. 5*b*, right), which both originate from the inactive adenylation domain (IAD). The similarity in AMP coordination between our Uba1–Ub(a) structure and MoaB–MoaD emphasizes the evolutionarily conserved mechanism of acyladenylate formation.

After activation of ubiquitin, the next step in the ubiquitylation cascade is the binding of an E2 ubiquitin-conjugating enzyme (Ubc) to the E1, which is doubly loaded with ubiquitin, thus yielding a quaternary complex. Olsen and Lima solved the structure of a ternary E1–E2–Ub(a) complex by

introducing a disulfide linkage between the active-site cysteine of Ubc4 (Cys85) and the catalytic cysteine of Uba1 (Cys593) from *S. pombe* (Fig. 4*c*). Ubc4 contacts the SCCH and the UFD domains of *Sp*Uba1 as well as the crossover loop and the ubiquitin located at the AAD (Olsen & Lima, 2013). To illustrate a quaternary E1–E2–Ub(a)–Ub(t) complex, the structure of Uba1–Ubc4–Ub(a) (PDB entry 4ii2) has been superposed with the Uba1–Ub(a)–Ub(t) structure from *S. cerevisiae* described in this study. This can be accomplished either by including the thioester-bound Ub of *S. cerevisiae* into the *Sp*Uba1–Ubc4–Ub structure (option 1, Fig. 6*a*) or by positioning *S. pombe* Ubc4 in the *S. cerevisiae* Uba1–Ub(a)–Ub(t) complex (option 2, Fig. 6*c*). In both models the thioester-linked ubiquitin generated a joint interface area with Ubc4 of ∼300 Å^2 and, irrespective of option 1 or 2, involves almost the same amino acids in Ubc4 and Ub(t).

Option 1 revealed that Ub(t) fits nicely into the Uba1–Ubc4 structure of *S. pombe* (Figs. 6*a* and 6*b*), only causing clashes between the side chains of Asp87 and Asp117 of Ubc4 and Arg74 and Gly76 of Ub(t), respectively. These amino acids might adopt slightly different positions in the structure of the quaternary complex. In general, Ub(t) seems to be in a position favouring its fast transfer to an E2 enzyme without the additional need for a Ub(t) displacement away from the SCCH domain to the 'front' of this complex as was suggested previously (Olsen & Lima, 2013). In our models of the quaternary complex the interface between Ubc4 and Ub(t) buries a surface area of about 7% of Ub(t) (*PDBePISA*; Krissinel & Henrick, 2007). Therefore, Ub(t) might contribute in this position to E2 binding by providing a further docking site after rotation of the UFD.

While Ub(t) of *S. cerevisiae* fits into the structure of *Sp*Uba1–Ubc4/Ub, the insertion of *Sp*Ubc4 (option 2) into *Sc*Uba1–Ub(a)–Ub(t) (Fig. 6*c*) led to overlaps between Ubc4 and residues 776–787 of the Uba1 SCCH domain (Fig. 6*d*). These amino acids correspond to the Cys CAP loop (residues 765–786), part of the SCCH domain (Figs. 2*b*, 2*d* and 6*d*), which covers the E1 active-site cysteine in Uba1 (Lee & Schindelin, 2008; Olsen & Lima, 2013). This region displays high mobility in all published Uba1 structures to date, leading for example in the structure from *S. cerevisiae* to the absence of amino acids 788–794 and of residues 770–782 in the Uba1–Ub structures of *S. pombe* (PDB entry 4ii3). Olsen and Lima showed that upon binding of the E2 enzyme to SCCH of Uba1, the Cys CAP loop becomes even more disordered and is therefore not visible, thus enabling a closer contact of the E2 active-site cysteine with Cys593 of *S. pombe* Uba1 (Fig. 6*b*). In our structure, in which Ub(t) is covalently linked to Cys600, this loop still partially masks the catalytic cysteine and its surrounding residues (Fig. 6*d*). Therefore, it remains unclear whether the Cys CAP loop protects the active site during selected steps of the catalytic cycle or provides an additional platform for E2 binding as was suggested previously (Olsen & Lima, 2013). In option 2 the common interface between Ubc4 and the UFD domain of *Sc*Uba1 does not exist since the UFD in our structure

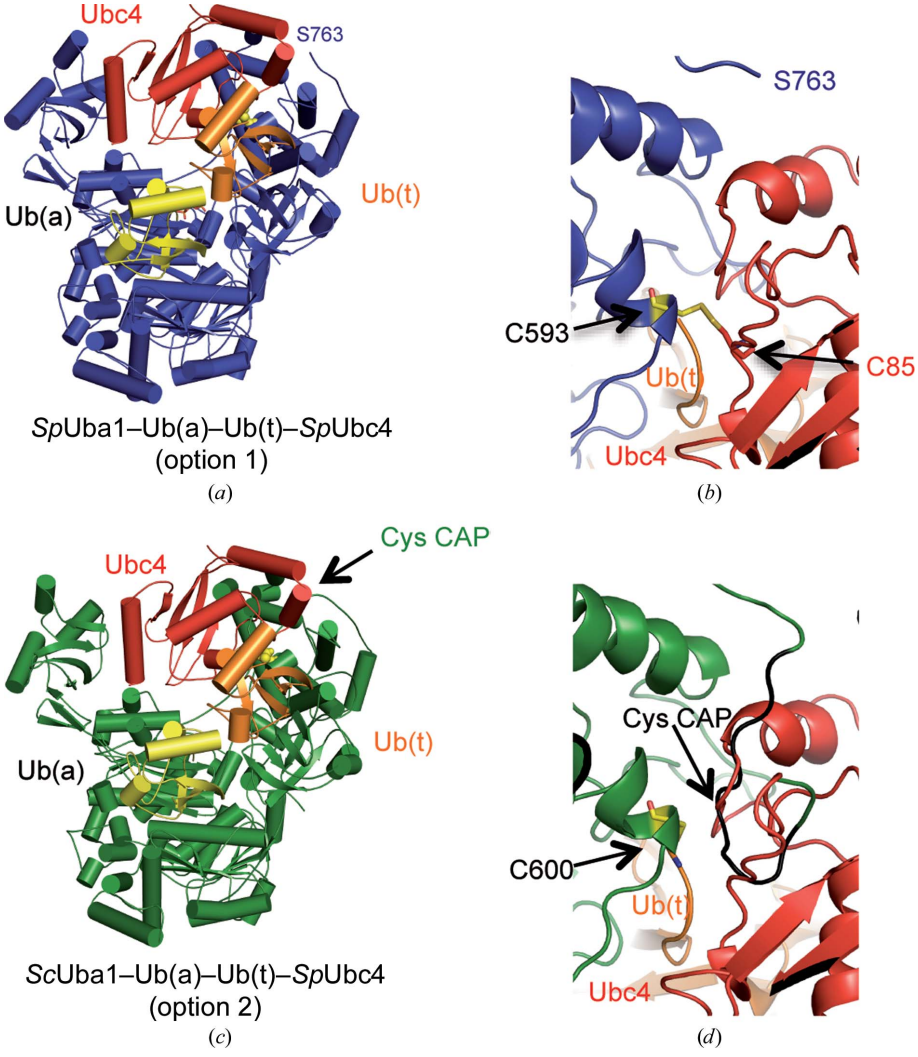

Figure 6
Models of the quaternary Uba1–Ubc4–Ub(a)–Ub(t) complex. Two options for a quaternary Uba1–Ubc4–Ub(a)–Ub(t) complex have been modelled with chains coloured as introduced in Fig. 4. (*a*) Ub(t) of *S. cerevisiae* after superposition of doubly loaded Uba1 onto the Uba1–Ub(a)–Ubc4 structure of *S. pombe* (option 1). (*b*) Close-up view of the Cys CAP loop region according to option 1. The Cys CAP loop (residues 764–786, not visible) is disordered, thus enabling a closer contact of the E2 active-site cysteine Cys85 to Cys593 of Uba1. (*c*) Ubc4 of *S. pombe* docked onto doubly loaded Uba1 from *S. cerevisiae* (option 2). (*d*) Close-up view of the clashes between Ubc4 and Uba1 in the Cys CAP region (residues 776–787 in black) as present in the model corresponding to option 2.

assumes the distal conformation (Fig. 6*c*). This aspect of the model again corroborates the necessity of a rotational motion of the UFD domain (Lee & Schindelin, 2008; Huang *et al.*, 2007; Olsen & Lima, 2013).

The structure presented here provides an additional snapshot along the E1-catalysed reaction cycle. We were able to visualize the formation of the ubiquitin-acyladenylate at the AAD together with the covalent attachment of a second ubiquitin to the active-site cysteine by X-ray crystallography. Model-building studies suggest that the covalently attached ubiquitin moiety together with the UFD and SCCH domains provide a platform for the recruitment of E2 enzymes, which are brought into close spatial proximity of the E1 active-site cysteine by a rotation of the UFD–E2 assembly.

This work was supported by the Deutsche Forschungsgemeinschaft (Rudolf Virchow Center for Experimental Biomedicine, FZ 82; HS) and Schi 425/6-1. We thank the ESRF in Grenoble and the BESSY in Berlin for synchrotron beam time and support. We are grateful to Dr Johannes Schiebel for data collection and to Drs Petra Hänzelmann and Daniela Schneeberger for critical reading of the manuscript.

References

Adams, P. D. *et al.* (2010). *Acta Cryst.* D**66**, 213–221.
Burroughs, A. M., Iyer, L. M. & Aravind, L. (2009). *Proteins*, **75**, 895–910.
Burroughs, A. M., Iyer, L. M. & Aravind, L. (2012). *Methods Mol. Biol.* **832**, 15–63.
Ciechanover, A., Heller, H., Katz-Etzion, R. & Hershko, A. (1981). *Proc. Natl Acad. Sci. USA*, **78**, 761–765.
Duda, D. M., Walden, H., Sfondouris, J. & Schulman, B. A. (2005). *J. Mol. Biol.* **349**, 774–786.
Emsley, P. & Cowtan, K. (2004). *Acta Cryst.* D**60**, 2126–2132.
Evans, P. (2006). *Acta Cryst.* D**62**, 72–82.
Goldberg, A. L. (2007). *Biochem. Soc. Trans.* **35**, 12–17.
Haas, A. L. & Rose, I. A. (1982). *J. Biol. Chem.* **257**, 10329–10337.
Haas, A. L., Warms, J. V., Hershko, A. & Rose, I. A. (1982). *J. Biol. Chem.* **257**, 2543–2548.
Haas, A. L., Warms, J. V. & Rose, I. A. (1983). *Biochemistry*, **22**, 4388–4394.
Hänzelmann, P., Schäfer, A., Völler, D. & Schindelin, H. (2012). *Methods Mol. Biol.* **832**, 547–576.
Huang, D. T., Hunt, H. W., Zhuang, M., Ohi, M. D., Holton, J. M. & Schulman, B. A. (2007). *Nature (London)*, **445**, 394–398.
Kabsch, W. (1976). *Acta Cryst.* A**32**, 922–923.
Kabsch, W. (1978). *Acta Cryst.* A**34**, 827–828.
Kabsch, W. (2010). *Acta Cryst.* D**66**, 125–132.
Kim, R., Yokota, H. & Kim, S.-H. (2000). *Anal. Biochem.* **282**, 147–149.
Krissinel, E. & Henrick, K. (2004). *Acta Cryst.* D**60**, 2256–2268.
Krissinel, E. & Henrick, K. (2007). *J. Mol. Biol.* **372**, 774–797.
Lake, M. W., Wuebbens, M. M., Rajagopalan, K. V. & Schindelin, H. (2001). *Nature (London)*, **414**, 325–329.
Lee, I. & Schindelin, H. (2008). *Cell*, **134**, 268–278.
Lehmann, C., Begley, T. P. & Ealick, S. E. (2006). *Biochemistry*, **45**, 11–19.
Lois, L. M. & Lima, C. D. (2005). *EMBO J.* **24**, 439–451.
McCoy, A. J., Grosse-Kunstleve, R. W., Adams, P. D., Winn, M. D., Storoni, L. C. & Read, R. J. (2007). *J. Appl. Cryst.* **40**, 658–674.
Metzger, M. B., Hristova, V. A. & Weissman, A. M. (2012). *J. Cell Sci.* **125**, 531–537.
Olsen, S. K., Capili, A. D., Lu, X., Tan, D. S. & Lima, C. D. (2010). *Nature (London)*, **463**, 906–912.
Olsen, S. K. & Lima, C. D. (2013). *Mol. Cell*, **49**, 884–896.
Petroski, M. D. (2008). *BMC Biochem.* **9**, S7.
Pickart, C. M. & Rose, I. A. (1985). *Prog. Clin. Biol. Res.* **180**, 215.
Rajagopalan, K. V. (1997). *Biochem. Soc. Trans.* **25**, 757–761.
Reinstein, E. & Ciechanover, A. (2006). *Ann. Intern. Med.* **145**, 676–684.
Rudolph, M. J., Wuebbens, M. M., Rajagopalan, K. V. & Schindelin, H. (2001). *Nature Struct. Biol.* **8**, 42–46.
Schulman, B. A. & Harper, J. W. (2009). *Nature Rev. Mol. Cell Biol.* **10**, 319–331.
Veen, A. G. van der & Ploegh, H. L. (2012). *Annu. Rev. Biochem.* **81**, 323–357.
Walden, H., Podgorski, M. S., Huang, D. T., Miller, D. W., Howard, R. J., Minor, D. L. Jr, Holton, J. M. & Schulman, B. A. (2003). *Mol. Cell*, **12**, 1427–1437.